(Preprint) AAS 14-285

NUCLEAR EXPLOSION ENERGY COUPLING MODELS FOR OPTIMAL FRAGMENTATION OF ASTEROIDS

Pavithra Premaratne[*], Ben J. Zimmerman[†], Christian Setzer[‡], Jake Harry[§], and Bong Wie[¶]

This paper examines both Tillotson and Jones-Wilkins-Lee (JWL) based energy coupling models, that are often used by various hydrodynamic codes for simulating the effects of high energy explosives. A subsurface nuclear explosion has been known to be 20 times more efficient than a contact burst. Both in-house and commercial AUTODYN hydrodynamic codes are used to validate such a known high efficiency factor of subsurface nuclear explosions. Several test cases are presented, illustrating good agreement with the AUTODYN software. In addition, a new approach for modeling high energy explosives is presented and compared with analytic results and simulations by AUTODYN. Our preliminary results indicate a maximum efficiency factor of only 11 when comparing subsurface versus contact blasts.

INTRODUCTION

Responding to threats from near-Earth objects (NEOs) with short warning times is a complex problem. Late detection of such threats provides a short response window, limiting most of the conventional, non-nuclear approaches. A nuclear explosive device (NED) is the only viable option against such impact threats with short warning times. However, this option needs thorough examination prior to execution, by identifying mission critical parameters which ensure the complete disruption of the asteroid. Determination of the NED yield and energy coupling to the target body is necessary to ensure mission success. A low energy coupling may result in partial fragmentation of the NEO due to its rubble like nature, increasing the probability of a collision with the Earth.

The Asteroid Deflection Research Center (ADRC) at Iowa State University has dedicated its research efforts to identify and answer such issues. A HAIV (Hypervelocity Asteroid Intercept Vehicle) concept is under development, which utilizes a kinetic impact followed by a nuclear subsurface explosion. The HAIV concept is being developed for NASA Innovative Advanced Concepts (NIAC) Phase 1 and 2 studies.[3,4,5,6]

[*]Graduate Research Assistant, Asteroid Deflection Research Center, Department of Aerospace Engineering, 1200 Howe Hall,Ames, IA-50011.

[†]Graduate Research Assistant, Asteroid Deflection Research Center, Department of Aerospace Engineering, 1200 Howe Hall, Ames, IA 50011.

[‡]Undergraduate Research Assistant, Asteroid Deflection Research Center, Department of Aerospace Engineering, 1200 Howe Hall, Ames, IA 50011.

[§]Undergraduate Research Assistant, Asteroid Deflection Research Center, Department of Aerospace Engineering, 1200 Howe Hall, Ames, IA 50011.

[¶]Vance Coffman Endowed Chair Professor, Asteroid Deflection Research Center, Department of Aerospace Engineering, 1200 Howe Hall, Ames, IA 50011.

This paper provides an extension to the hydrodynamic modeling work completed in the past, which used a graphics processing unit (GPU) accelerated planar smooth particle hydrodynamic (SPH) algorithm. A new explicit hydrodynamic software called AUTODYN by ANSYS is currently being utilized to model and optimize the efficiency of the HAIV approach. AUTODYN provides both Lagrangian and Eulerian modeling frameworks in 2D and 3D, and allows visualization of solutions in real time. In addition, a validated material library is included for accurate material properties. AUTODYN also aids in simulation setup time by including geometry manipulation tools and built-in grid generators. Additionally, this paper investigates another new approach, which utilizes high-order (order of accuracy 3^{rd} or higher) numerical methods developed in computational fluid dynamics (CFD). The correction procedure via reconstruction (CPR), developed by Huynh[12] and extended by Wang,[15] is implemented and tested against both analytical and AUTODYN solutions in one and two-dimensional blast wave problems.

METHODS

This section discusses the modeling of hydrodynamic simulations and the basic formulation of the SPH and CPR methods. The data for material models was extracted from previous works of literature in the field and documentation provided by ANSYS. The explosive device chosen in most simulations is Trinitrotoluene (TNT). Energy coupling is modeled via two methods: Direct energy deposition and Jones-Wilkins-Lee (JWL) equation of state. The direct energy deposition model was initially used in the in-house GPU SPH algorithm and was implemented in AUTODYN for comparison. The implemented CPR method currently uses only the direct energy deposition model for simulations.

Blast Optimization and Energy Deposition

A series of studies are currently underway to investigate the energy coupling by the explosive to the asteroid. The energy deposition schemes below are tested and employed for a wide variety of 2D and 3D SPH simulations presented in this paper.

Direct Energy Deposition (DED). Upon specifying a yield for the payload (e.g., 100 kilotons), total energy of the device is calculated in Joules using the specific internal energy of TNT. The specific internal energy of nodes is then calculated by dividing the total energy by the nodal mass. The specific internal energy calculated is an input to the simulation as an initial condition. This method produces an isotropic explosion, converting a fraction of its internal energy to kinetic energy, which will be coupled to the target body. Material properties are governed by Tillotson equation of state throughout the simulation for both target body and the explosive device. The Tillotson equation was also used in the in-house GPU SPH algorithm, but is not yet implemented in the CPR method.

JWL Equation with a Detonation Mechanism. A specific detonation mechanism (point source or line source) along with an initiation time governs the energy distribution and coupling. These simulations and explosion models are currently under testing with multiple material models for the target body. Rock material characteristic models, which encapsulate the brittle and rubble like nature, are implemented to further test the blast dynamics. Optimized results will be used in calculating an efficiency factor for a subsurface explosion compared to a surface blast. The 20 times efficiency factor was extracted from a study published by National Research Council (NRC) based on a series of tests conducted by the Department of Energy.[10] According to the empirical curves presented in Figure 1, subsurface detonations yield an increase to the energy coupling efficiency when compared

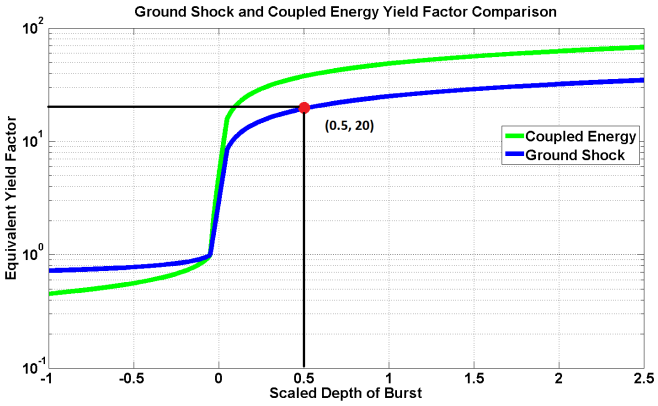

Figure 1. Efficiency Plot

to surface blasts. The scaled depth-of-burst (DOB) used in Figure 1 is defined as

$$DOB = \frac{x}{Y^{(\frac{1}{3})}} \tag{1}$$

where x is the buried depth and Y is the device yield.

Validating the above mentioned efficiency factors will aid us in the design process when determining required impact velocity for the kinetic impactor and required mass of the detonation payload, thus improving overall mission efficiency. Energy coupling to the target object is determined by the following factors:[9] material characteristics of the target, target resolution, blast modeling scheme and simulation framework (e.g., FEM/SPH), and buried depth of the explosive device.

SPH Formulation

The SPH method is a Lagrangian particle physics method, initially used to solve astrophysics problems. It is formulated with the basic fluid dynamic equations smoothed over a kernel function W for a calculated or specified smoothing length. The kernel function, usually specified as a cubic spline, modifies the basic fluid dynamic equations via averaging to obtain the following conservation of mass, momentum, and energy equations (the first equation defines the velocity vector)

$$\begin{aligned}
\frac{D\mathbf{x}_i}{Dt} &= \mathbf{v}_i \\
\frac{D\rho_i}{Dt} &= \sum_{j=1}^{N} m_j(\mathbf{v}_i - \mathbf{v}_j)\cdot\nabla_i W_{ij} \\
\frac{D\mathbf{v}_i}{Dt} &= \sum_{j=1}^{N} m_j(\frac{p_i}{\rho_i^2} + \frac{p_j}{\rho_j^2} + \mu_{ij})\nabla_i W_{ij} \\
\frac{De_i}{Dt} &= \frac{1}{2}\sum_{j=1}^{N} m_j(\frac{p_i}{\rho_i^2} + \frac{p_j}{\rho_j^2} + \mu_{ij})(\mathbf{v}_i - \mathbf{v}_j)\cdot\nabla_i W_{ij}
\end{aligned} \tag{2}$$

Variable definitions can be found in the Notation section. Numerical integration of the above equations can be performed by using a leap frog or a Runge Kutta method. AUTODYN also incorporates

an adaptive time step calculation along with density limiters to ensure the robustness of the simulation. Smoothing length of the simulation is updated with each time step for faster and accurate results.[1]

CPR Method

The CPR method was developed to improve the efficiency of other high-order methods previously developed for CFD simulations. These include the discontinuous Galerkin (DG),[13,14,16] spectral volume (SV),[19,22] staggered grid (SG) multi-domain,[17,18] and spectral difference (SD)[20,21] methods. The CPR method solves the following hyperbolic equation law

$$\frac{\partial \mathbf{q}}{\partial t} + \frac{\partial \mathbf{f}}{\partial x} + \frac{\partial \mathbf{g}}{\partial y} = 0 \tag{3}$$

where $\mathbf{f}$ and $\mathbf{g}$ are the flux vectors. The state vector, $\mathbf{q} \in P^k(V_i)$ ($\mathbf{q}$ belongs to the space of polynomials degree k on element i of volume V), is

$$\mathbf{q} = \begin{bmatrix} \rho \\ \rho u \\ \rho v \\ e \end{bmatrix} \tag{4}$$

where ρ is the density, u and v are the velocities along x and y directions, and e is the total energy per unit volume. The inviscid-flux vectors are

$$\mathbf{f} = \begin{bmatrix} \rho u \\ p + \rho u^2 \\ \rho uv \\ u(e+p) \end{bmatrix} \qquad \mathbf{g} = \begin{bmatrix} \rho v \\ \rho uv \\ p + \rho v^2 \\ v(e+p) \end{bmatrix} \tag{5}$$

where the pressure, under the ideal gas law, is $p = (\gamma - 1)(e - \frac{1}{2}\rho(u^2 + v^2))$. The CPR formulation closely follows DG to a point. The derivation changes the formulation from an integral one (as completed in DG), to a differential formulation. Full derivation of the method[15] results in a "penalty" term for the normal flux difference across element interfaces. A "correction field", $\boldsymbol{\delta}$, forms a "lifting operator" which results in the following equation

$$\frac{\partial \mathbf{q}_{i,j}}{\partial t} + \Pi_j \left[\frac{\partial \mathbf{f}_i}{\partial x} + \frac{\partial \mathbf{g}_i}{\partial y} \right] + \boldsymbol{\delta}_{i,j} = 0 \tag{6}$$

where i and j denote each element and solution point respectfully. Unlike the SPH method, the CPR method requires a computational grid, with solution points set interior to each element. Solution points are chosen to coincide with the elements interfaces and flux points, reducing interpolation costs. While this simplifies the derivation, the flux may not necessarily reside in the space $P^k(V_i)$, since the flux derivative is approximated by polynomials of degree k or less. Hence, the divergence is projected into the proper space via the projection term Π_j. Formulation of the correction field as well as correction coefficients have already been completed.[23] Current implementation uses quadrilateral elements, resulting in an efficient calculation of the correction field, since the operations are completed in a one-dimensional manner.

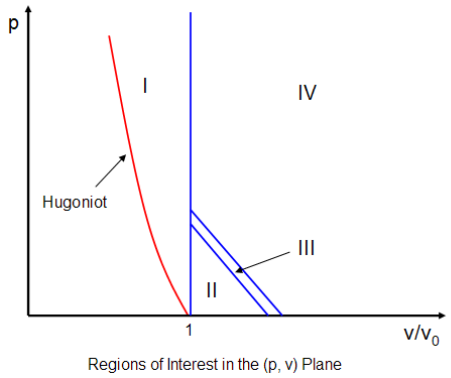

Figure 2. Tillotson Equation of State (Image courtesy of AUTODYN Manual 14.5)

Material Modeling

A multitude of material modeling options consisting of different equations of states, strength, and failure models are under investigation in order to capture the accurate material characteristics during the hypervelocity impact and nuclear sub-surface explosion. The NED yield is currently modeled via TNT material properties. The Jones-Wilkins-Lee (JWL) equation of state is specified for the explosive material, while the target is modeled by Tillotson equation of state. Capturing the material behavior is crucial, as these characteristics determine the failure method, particle velocities, and energy coupling factors. Such parameters can be used to determine appropriate guidance parameters (e.g., impact angle and location) and the orbit determination of HAIV spacecraft. Sections below provide an overview of some equations of state that are currently under testing.

Tillotson EOS. The Tillotson equation of state is used to predict metallic material behavior during hypervelocity impacts. This equation addresses material phase changes, compressions, and expansions during the energy transfer. The Tillotson equation of state is defined for four regions located to the right of the Hugoniot curve. Figure 2 depicts the four regions that define shock compression.[2]

Within region I, the material is represented in a compressed state. The vertical line extends up to 1000 Mbar and the pressure is given as

$$P_1 = (a + \frac{b}{\omega_0})\eta\rho_0 e + A\mu + B\mu^2 \tag{7}$$

Region II defines material characteristics under shock due to energy that is less than the sublimation energy. The pressure here is

$$P_2 = (a + \frac{b}{\omega_0})\eta\rho_0 e + A\mu \tag{8}$$

At region III, the pressure is just the mean pressure between regions II and IV given by

$$P_3 = P_2 + \frac{(P_4 - P_2)(e - e_s)}{e_s\prime - e_s} \tag{9}$$

where $x = 1 - \frac{1}{\eta}$. Material parameters, such as a, b, α, β and e_0, are fitting parameters for the Tillotson equation of state. The parameter A is considered the Bulk Modulus and B represents the compressive term.[7]

Table 1. Shock Equation of State Properties

Parameter	Definition	Water
ρ_0	Initial Density	1000 kg/m^3
C	Sound Speed	18.0 (GPa)
γ_0	Gruneisen coefficient	0.5
a	Volume correction coefficient	0.0
S_1	Fitting coefficient	2.56
S_2	Fitting coefficient	1.986
S_3	Fitting coefficient	1.2268

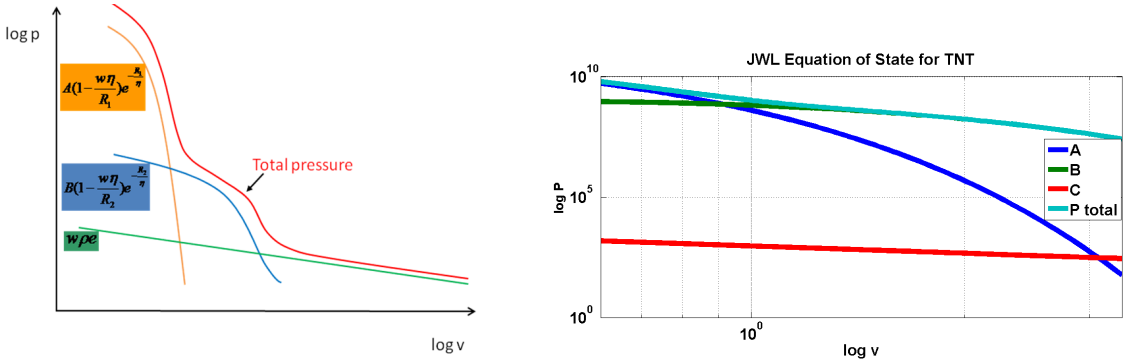

(a) General equation of state

(b) TNT equation of state

Figure 3. JWL Equation of State

Shock Equation of State. The shock equation of state was developed under empirical relations. The equation represents characteristics of underwater explosions. Definitions of parameters and respective values for water are given in Table 1, along with the pressure calculation described by

$$p = \frac{\rho_0 C^2 \mu [1 + (1 - \frac{\gamma_0}{2})\mu - \frac{a}{2}\mu^2]}{[1 - (S_1 - 1)\mu - S_2 \frac{\mu^2}{\mu+1} - S_3 \frac{\mu^3}{(\mu+1)^2}]^2} + (\gamma_0 + a\mu)e \tag{10}$$

where $\mu = \frac{\rho}{\rho_0} - 1$.

Jones-Wilkins-Lee (JWL) Equation of State. This equation was developed from various empirical relationships obtained from experiments conducted with high energy explosives such as TNT. Pressure of the explosive gas is given by

$$p = A(1 - \frac{\omega\eta}{R_1})e^{-\frac{R_1}{\eta}} + B(1 - \frac{\omega\eta}{R_2})e^{-\frac{R_2}{\eta}} + \omega\eta\rho_0 e \tag{11}$$

where $A, B, R1, R2$ and ω are coefficients obtained from experiment and η represents density ratio between the gaseous products and original material. Specific internal energy of the material is denoted by e and ρ_0 is the initial density of the material. A graphical representation of the relationship between pressure and volume is given in Figure 3(a).[2] The JWL equation for TNT is shown in Figure 3(b),[2] where the three terms of Eq. (11) are plotted along with total pressure.

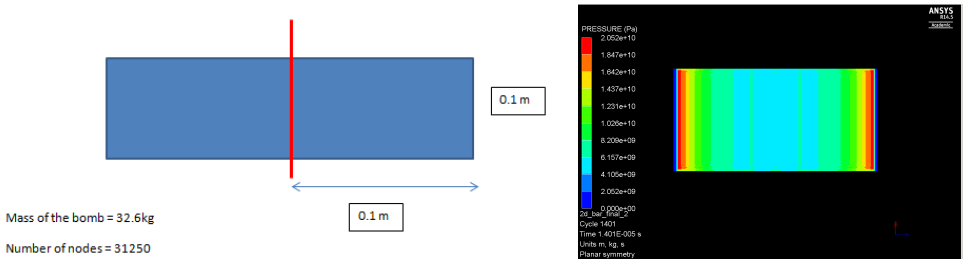

Figure 4. Setup and Result

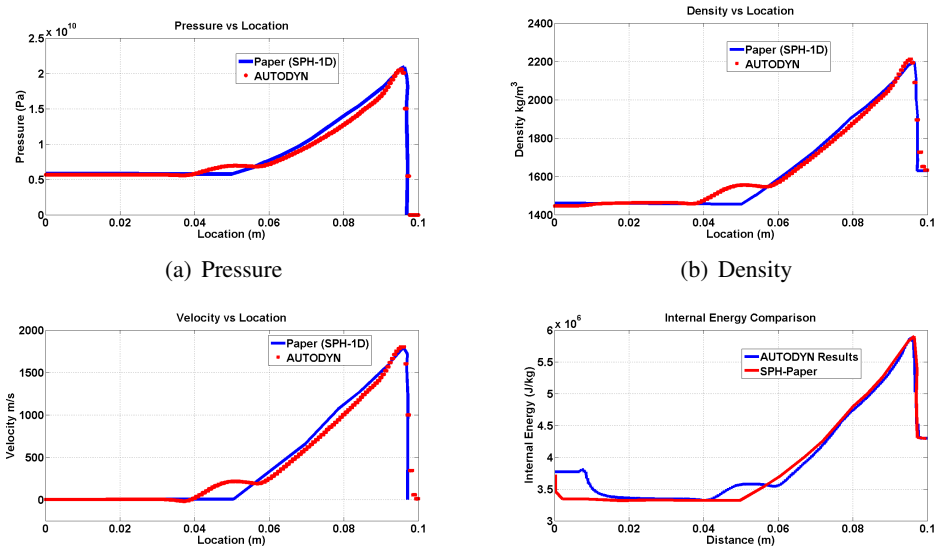

(a) Pressure (b) Density

(c) Velocity (d) Internal energy

Figure 5. 1D TNT Simulation

CODE VALIDATION

Detonation of 1D Bar of TNT (AUTODYN)

1D bar of TNT was detonated from the middle, allowing the shock to propagate symmetrically to the end of the explosive device. Pressure, velocity, and density were recorded from the axis of symmetry to the end of the bar at 14 microseconds simulation time. The simulation setup is shown in Figure 4. Pressure, density, velocity and internal energy results extracted from the AUTODYN solution given above are compared with the SPH results.[1] Simulated results agree with the curves presented in the paper in a very satisfactory manner. A small peak in AUTODYN results can be observed where the change in slope occurs. This could be due to a modeling difference (grid resolution or smoothing length) that can only be identified by comparing both algorithms.

In the absence of another material interface, the shock wave reflects from the edges and travel towards the center of the device. Total energy in the explosive remains as internal energy during the initial shock propagation. During the second stage of the detonation process, most of the internal energy transforms into kinetic energy due to rapid gas expansion. In the presence of another material, such as water, air or rock, the shock wave travels to the material, where a refraction wave

occurs, whose magnitude depends on refraction index of the given material. The shock wave may deteriorate depending on the material characteristics, and some of the shock energy is lost through material interfaces and in fragmentation.

Sods Shock Tube (CPR)

Prior to comparing the CPR method to the AUTODYN program, the implementation must be verified, specifically the ability to capture shock waves. Due to the nature of high-order methods, they become oscillatory and unstable in regions of high gradients (shocks). To remedy this problem, artificial viscosity or slope limiting are frequently used. Artificial viscosity requires specifying the amount of viscosity to add. Adding too much will cause the shocks to become smeared and inaccurate, but too little and instability occurs. In addition, second order derivatives are introduced, which need to be discretized for the given numerical formulation. Slope limiting is more straightforward, but the high-order accuracy of the method is lost (as slope limiters are generally 1^{st} or 2^{nd} order). The results presented use a slope limiter coupled with a shock detector similar to that presented by Persson and Peraire,[24] with slight modification. The solution (of order k) is defined as

$$\alpha = \sum_{i=1}^{n(k)} \alpha_i \phi_i \tag{12}$$

where $n(k)$ is the number of expansion terms and ϕ_i are basis functions. Next, define a solution only including terms up to $n(k-1)$ such that

$$\hat{\alpha} = \sum_{i=1}^{n(k-1)} \alpha_i \phi_i \tag{13}$$

then, a indicator for smoothness can be defined as

$$J_i = \frac{(\alpha - \hat{\alpha}, \alpha - \hat{\alpha})_i}{(\alpha, \alpha)_i} \tag{14}$$

where $(*, *)_i$ is defined as the standard inner product in element i. In this paper, evaluation of $\hat{\alpha}$ is completed via interpolation (the solution is interpolated to solution points a degree lower) instead of recomputing the high-order coefficients. This changes the scaling of J_i which is currently under investigation. To test the sensor, simulation of Sods shock tube with a standard minmod limiter is completed and compared to the analytic solution. The domain is discretized from $[0, 1]$ with $\rho = 1.0$ and $p = 1.0$ for $x > 0.5$ and $\rho = 0.125$ and $p = 0.1$ for $x < 0.5$ with $u = 0$ everywhere. At time $t = 0.2$ the density and pressure are compared against the analytic solution. Excellent agreement is shown between the pressure and density.

1D Interacting Blast Waves (CPR)

To further test the shock capturing of the high-order method, another one-dimensional case is considered. The domain is discretized from $[0, 1]$ with reflecting boundaries. From $0.1 < x < 0$ the pressure is $p = 1000$, while from $1.0 < x < 0.9$ the pressure is $p = 100$. The density and velocity are $\rho = 1.0$ and $u = 0$ everywhere. This causes two blast waves to eventually collide, creating high gradients and providing an excellent test for the limiter and shock sensor implemented. Results for pressure and density are given at several time levels, with a comparison[25] of the density at

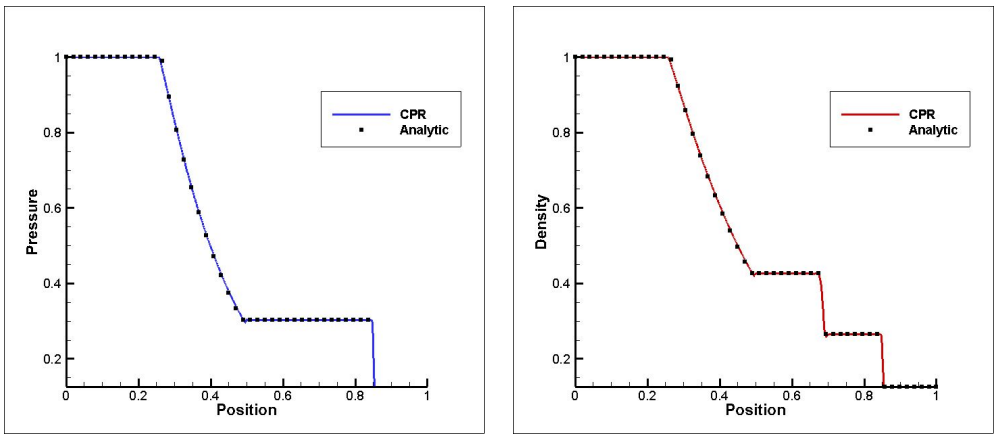

(a) Pressure comparison (b) Density comparison

Figure 6. Sods Shock Tube

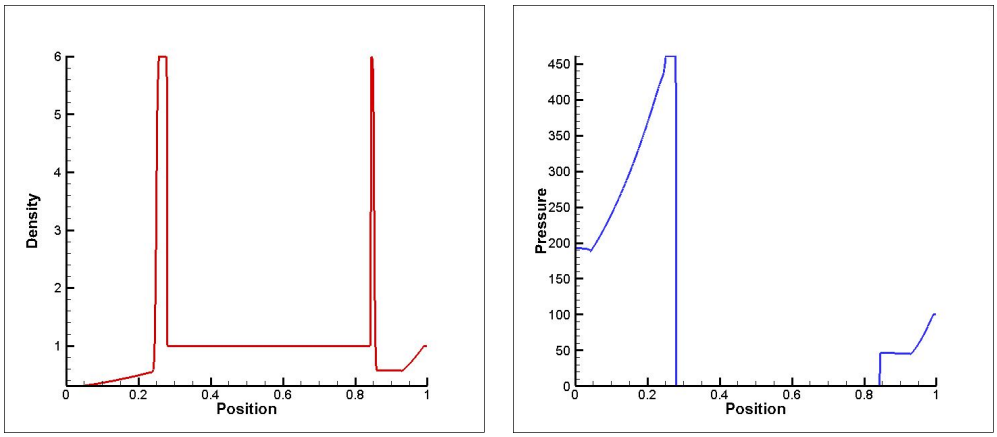

(a) Density (b) Pressure

Figure 7. Interacting Blast Waves at $\mathrm{t} = 0.0076$

the final time. Good agreement is illustrated in the density comparison. The shock detector and limiter appear to be working well together, as the solution is only limited near high gradients, while maintaining a high-order of accuracy throughout the remainder of the domain.

Underwater Explosion Simulations (UNDEX)

Water was introduced as a material interface in order to compare energy coupling results. Pressure data was obtained through a gauge point located at x = 0.25 m. A simulation setup is provided in Figure 10. Results obtained from AUTODYN shows a 0.5 ms lead. This lead was observable for both material models for water. This could be due to certain modeling schemes such as material boundary treatments and variable smoothing length schemes. An impact separation scheme and a variable scheme can be implemented in AUTODYN, but this makes the simulations prone to numerical instabilities. Implementation of a sound contact algorithm solves most of the lead-lag issues but introduces some stagnation in the material interfaces. Applying penalty schemes also

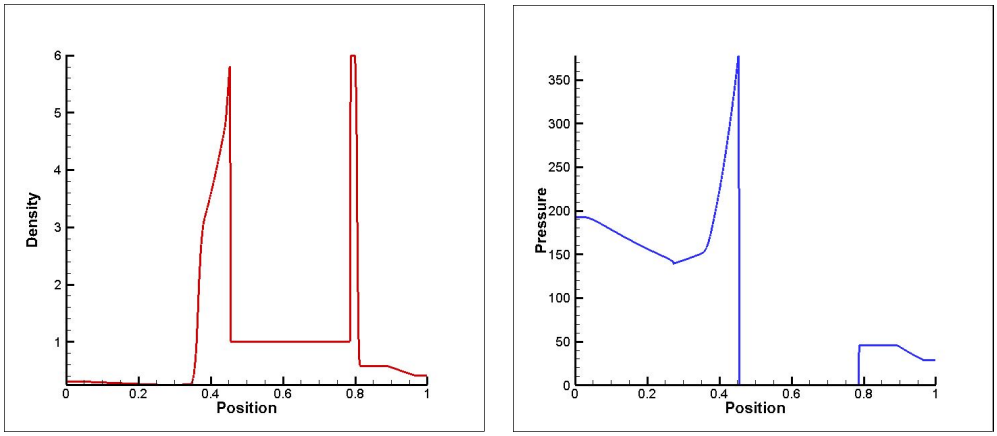

(a) Density (b) Pressure

Figure 8. Interacting Blast Waves at $t = 0.0152$

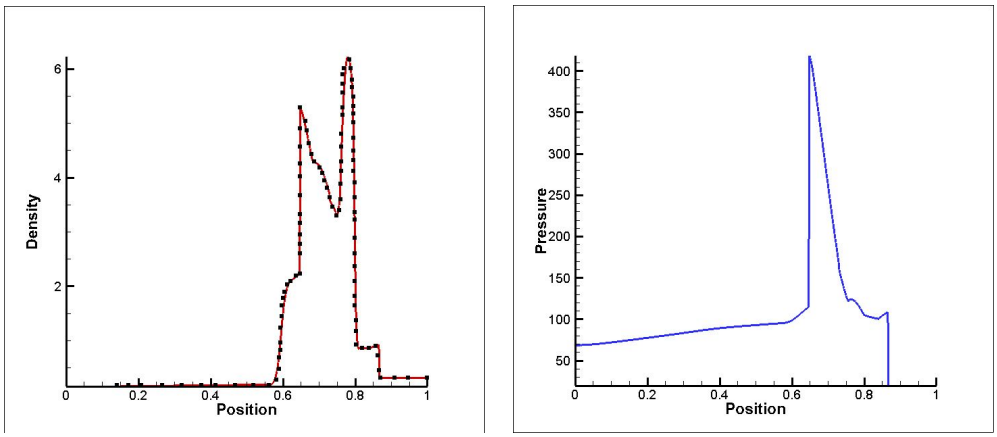

(a) Density with comparison[25] (b) Pressure

Figure 9. Interacting Blast Waves at $t = 0.0380$

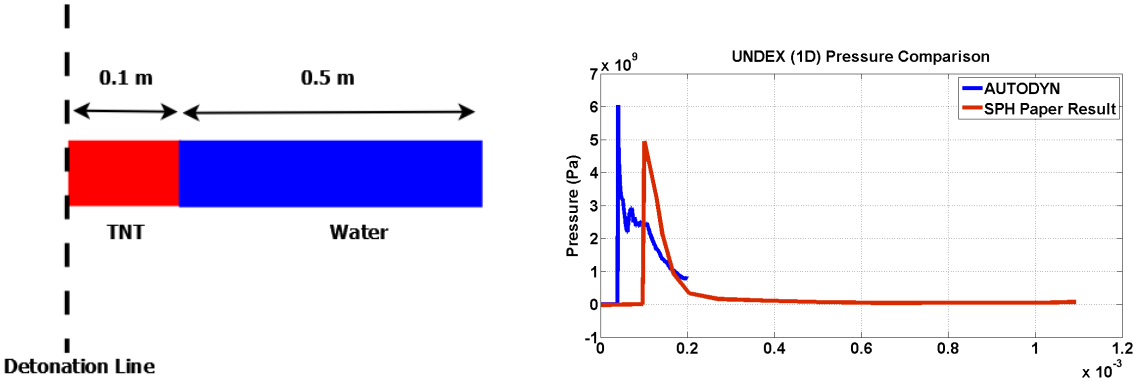

(a) Initial condition (b) Solution comparison

Figure 10. UNDEX 1D Setup

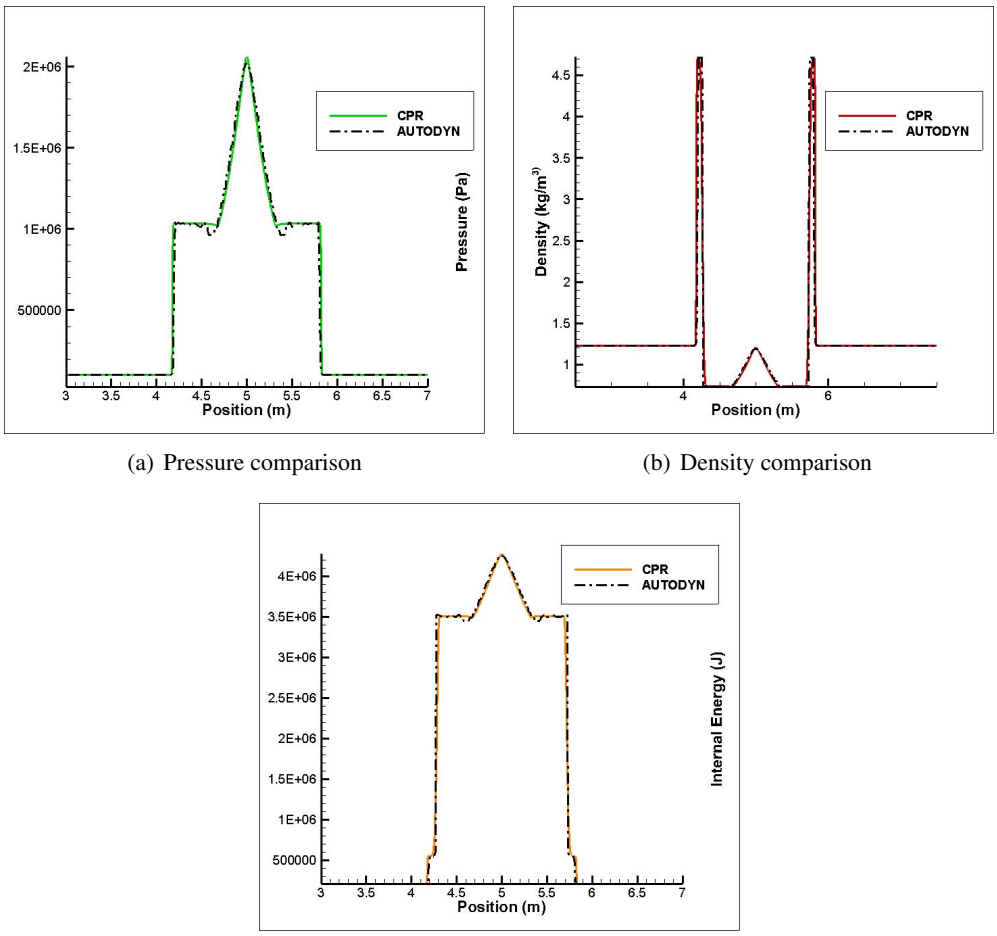

(a) Pressure comparison

(b) Density comparison

(c) Internal energy comparison

Figure 11. 1D air blast comparison.

improve material interface treatments.

AUTODYN and CPR Comparison 1D

A one-dimensional air blast test case was conducted to compare results from the methods. The domain was discretized from $[0, 10]$ with a specified energy source from $4.5 \leq x \leq 5.5$ of $e = 4.3 \times 10^6$ joules and $e = 2.0 \times 10^5$ joules throughout the remainder of the domain (corresponding to a 1 atm pressure). The density was set at $\rho = 1.225$ kg/m^3. As shown in Fig. 11, the pressure, density, and internal energy from AUTODYN and CPR match extremely well.

AUTODYN and CPR Comparison 2D

A two-dimensional case was also simulated to further test the methods. The initial conditions are similar to the 1D comparison test, only the blast is a circle with radius of 0.5. Comparing the pressure and density plots exhibit some differences. The AUTODYN simulation illustrates some spikes in the pressure solution not captured by the CPR method. Future work is needed to investigate this issue.

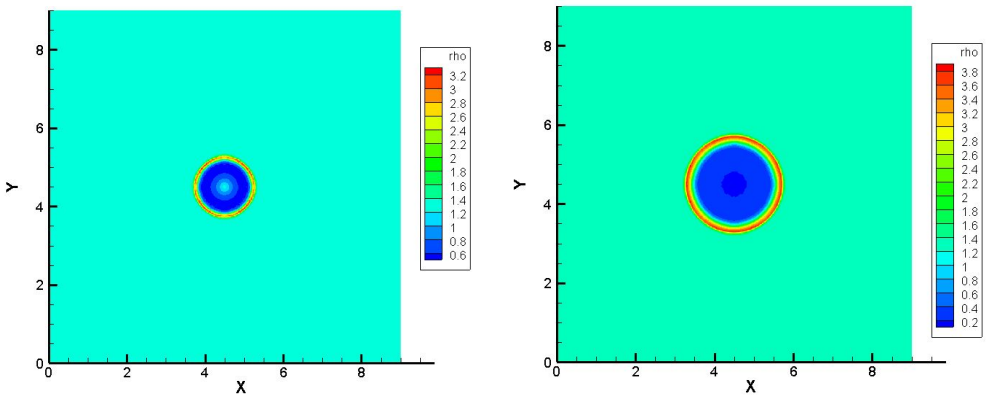

(a) Density at $t = 0.3$ μ seconds (b) Density at $t = 0.9$ μ seconds

Figure 12. 2D Air Blast Simulation (CPR)

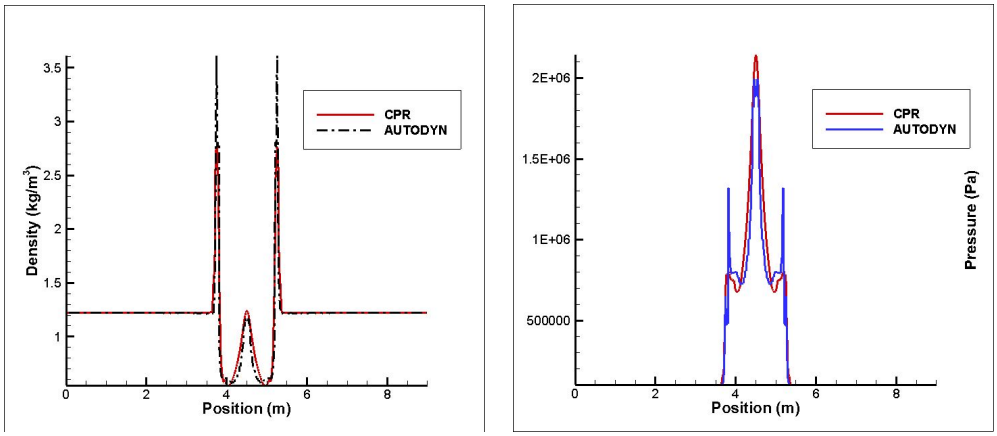

(a) Density at $t = 0.3$ μ seconds (b) Pressure at $t = 0.9$ μ seconds

Figure 13. 2D Air Blast Comparison

UNDEX 2D

A 2D axial symmetric simulation was also completed with the following setup. Axis of symmetry is shown in dash lines. A gauge point was set close to the boundary to record pressure. Mie-Gruneisen equation of state (EOS) was implemented to represent water. Recorded pressure response from the AUTODYN solution is compared with experimental results along with solutions obtained from another SPH algorithm.[11]

PRELIMINARY RESULTS AND ANALYSIS

2D Planar Simulations (JWL)

2D planar simulations were conducted for sub-surface and contact explosions. The explosive mass was 1.25 tons, governed by JWL equation of state, with a granite material target whose material parameters were governed by Tillotson equation of state. Simulation setup is shown in Figure 15. The material properties of granite and TNT are given in Table 2. AUTODYN material libraries

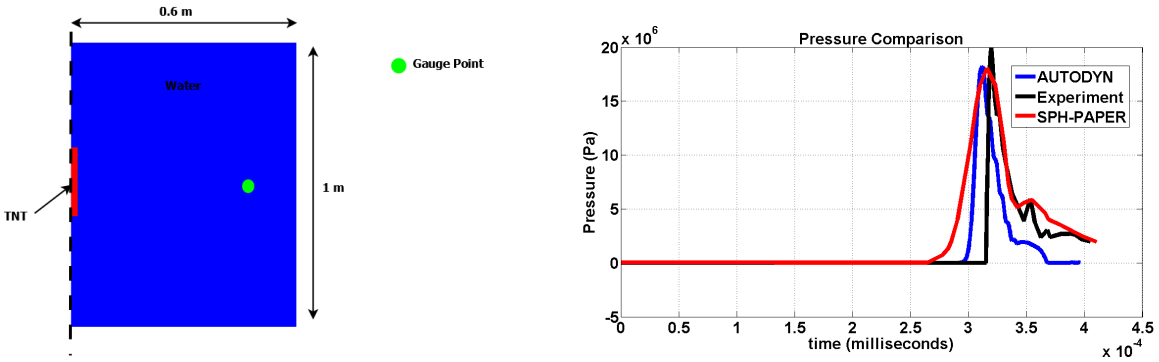

(a) Problem setup

(b) Pressure solution

Figure 14. UNDEX 2D Problem

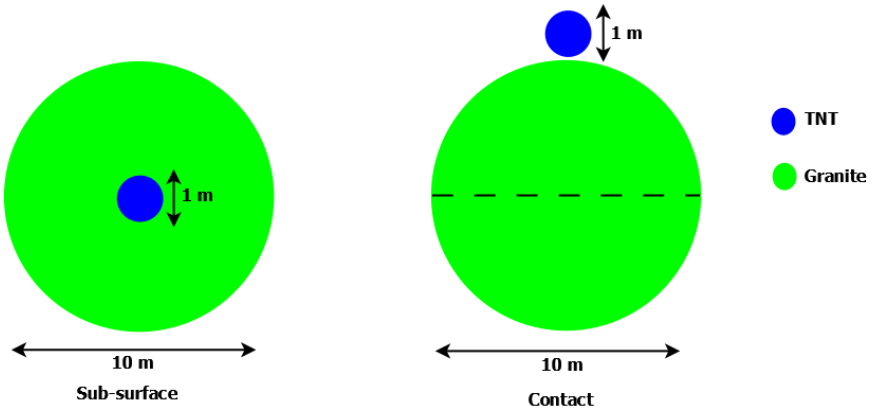

Figure 15. Planar Simulation Setup

were used to obtain TNT characteristics. Granite parameters were obtained from Marinova et al .[7] Pressure solutions obtained from the AUTODYN simulations are presented in Figure 16.

Once the device is triggered, explosive chemical energy, initially stored as internal energy, converts into kinetic energy, generating an isotropic displacement pattern. Percentages of this energy conversions are given in Table 4. The JWL model consists of a trigger time along with a point source detonation and assumes gaseous behavior (ideal gas) for the end products of the detonation, creating a rapid expansion. A point source was placed in the middle of the device as particles and an initial shock wave propagating from the center was observed upon triggering the device. Energy coupling to the target from the explosive device was compared between contact and subsurface explosion cases. The explosive efficiency of the subsurface explosion compared to contact scenario was computed to be around 7X.

2D Planar Simulations (DED)

These simulations consisted of a spherical target constructed from granite, modeled by the Tillotson equation of state. For the direct energy deposition method, the 1.25 ton device was modeled as high energy granite particles, still governed by Tillotson equation of state. A subsurface explosion with the device buried at the center of the target was simulated which was followed by a simulation

Table 2. Tillotson Equation of State Properties

Parameter	Granite
A	18.0(GPa)
B	18.0 (GPa)
a	0.5
b	1.3
α	5.0
β	5.0
e_0	16.0 MJ/kg
e_s	3.5 MJ/kg
e'_s	18.0 MJ/kg

Table 3. JWL Equation of State Properties

Parameter	Value
A	373.77(GPa)
B	3.7471(GPa)
R1	4.15
R2	0.9
ω	0.35
C-J Detonation velocity	6930 m/s
C-J Energy per unit volume	6(GJ/m^3)
C-J Pressure	21 (GPa)

of detonating the device slightly above the surface of the target. Energy coupling percentages were obtained for the granite target and presented in Table 5. Energy coupling from direct energy deposition is significantly lower than the coupling factors obtained by using JWL. Overall efficiency between sub-surface and contact simulations for DED method seems to be around 8X.

2D Axial Symmetric Solver

A axial symmetry solver was utilized to generate representative 3D solutions for the 2D planar simulations shown above. Both contact and sub-surface explosion simulations used JWL and DED detonation models. Pressure solutions for JWL are shown in Figure 18, while the DED solutions are in Figure 19. Energy coupling factors with respect to the total yield of the device for both cases are presented in Table 6.

For the subsurface explosion that utilizes JWL model, 46.8% of the total energy coupled to the asteroid remained as internal energy, while 53.2% caused nodal displacement as kinetic energy. A significant amount of energy (45% from the initial yield) remained in the explosive nodes as internal energy. As per the corresponding contact burst, 53% of the total energy coupled remained as internal energy. About 95% of the total yield of the device remained in the explosive particles as internal energy for the contact blast simulation. Efficiency of the subsurface blast with respect to contact explosion is computed to be 11X.

Table 4. Subsurface vs Contact - JWL

Simulation scenario	Kinetic Energy %	Internal Energy %	Total Energy Transferred %
Subsurface	46	54	47
contact explosion	50.0	50.0	7

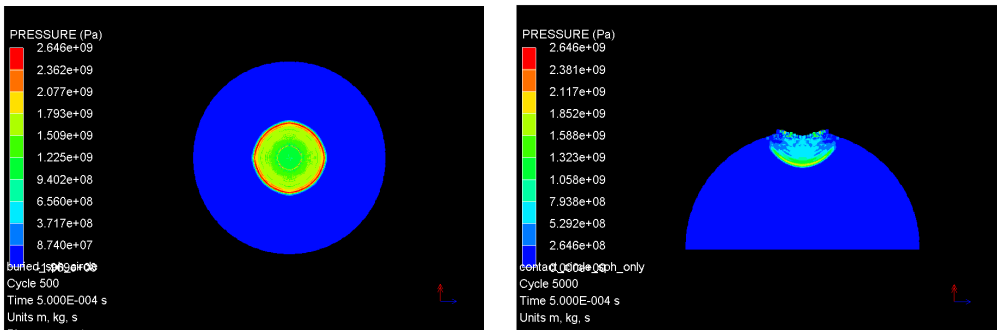

Figure 16. Pressure Solutions (JWL)

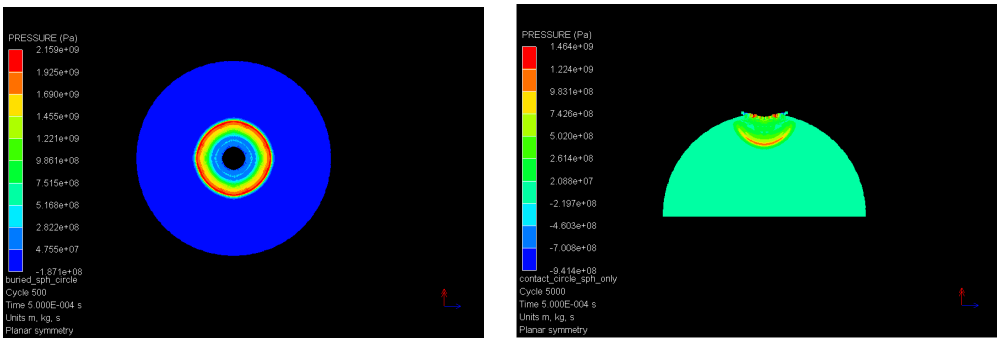

Figure 17. Pressure Solutions (DED)

As predicted in the 2D planar simulation, energy coupling seems to be significantly low for DED simulations when compared to the JWL simulations. Majority (roughly 73%) of the total yield of the device remained in the designated explosive nodes for the subsurface explosion, while 98% of the device energy didn't couple to the target during the contact blast. The explosive efficiency was calculated to be 10X.

According to these simulations, a significant percentage of energy remains in the explosive device. However, in an actual nuclear blast or a conventional explosive usage, a significant portion of total energy (35% to 45%) turns into thermal radiation.[8] The SPH framework employed by AUTODYN lacks thermal radiation modeling and therefore most of the energy in the explosive device remains in the assigned particles as internal energy. However, the JWL explosion model seems to be predicting higher energy coupling factors and efficiencies when compared to the direct energy deposition method.

Table 5. Subsurface vs Contact (DED)

Simulation Scenario	Kinetic Energy %	Internal Energy %	Total Energy Transferred from Explosives %
Subsurface	47.5	52.5	26
Contact Burst	53.7	46.3	3

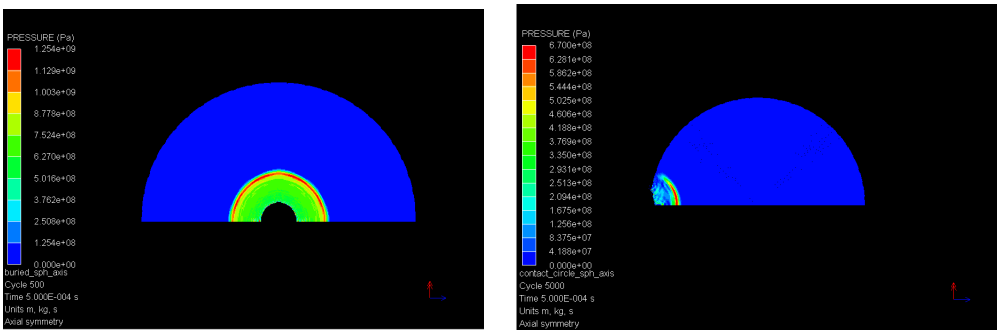

Figure 18. 2D Axial Symmetry (JWL): Before and After Subsurface Explosion

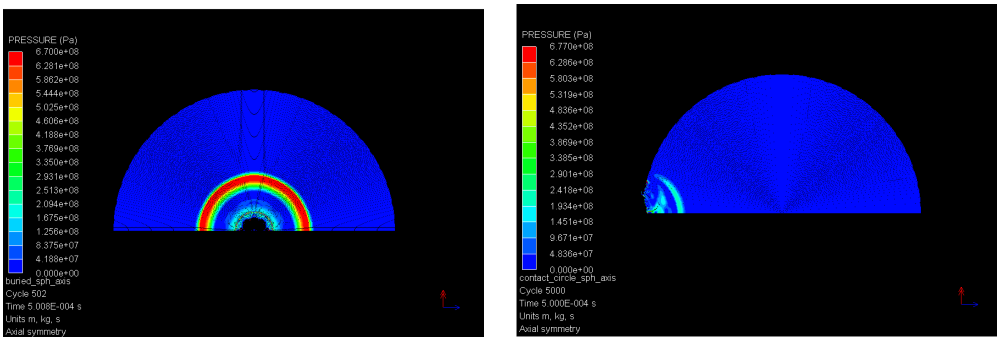

Figure 19. 2D Axial Symmetry (DED): Before and After Subsurface Explosion

CONCLUSIONS AND FUTURE WORK

The AUTODYN software demonstrates the ability to solve the problems as posted in this paper. Simulations under JWL explosion modeling showed higher energy coupling to the target bodies when compared against the direct energy deposition methods. More research is required to better understand the modeling differences between these two methods. Additionally, a new approach utilizing a high-order method, appears to not only capture shocks accurately, but exhibits good agreement with the AUTODYN software.

Future work is desired in understanding the modeling of the energy coupling and transfer to a target body through JWL models and energy sourcing. Different strength and material models should also be investigated, specifically rubble or porous materials. From multi-dimensional simulations, a comprehensive grid study should be completed to better understand the relationship between energy coupling and grid resolution. Simulations of ground shocks are also desired to validate the efficiency in Figure 1. Finally, development of the CPR method should continue, to better under-

Table 6. Subsurface vs Contact - Axis Symmetric

Simulation scenario	Kinetic Energy %	Internal Energy %	Total Energy Transferred from NED %
Subsurface (JWL) contact explosion (JWL)	53.2 47	46.8 53	55.4 4.75
Subsurface (DED) contact explosion (DED)	46.94 47	53.06 53	23.27 2

stand the modeling and having an additional numerical technique to solve such problems.

ACKNOWLEDGMENT

This research was supported by a NIAC Phase 2 study entitled "An Innovative Solution to NASA's NEO Impact Threat Mitigation Grand Challenge and Its Flight Demonstration Mission Design."

NOTATION

Table 7. Variable Definitions

Variable	Description
$\mathbf{x}$	Position vector
p	Pressure
ρ	Density
e	Internal energy
$\mathbf{v}$	Velocity vector
m	mass
μ	Artificial viscosity
i	Particle of interest
j	Index of the beighboring particle
N	Total number of neighbors

REFERENCES

[1] Liu, G.R. & Liu, M.B., "Smooth Particle Hydrodynamics: a mesh free particle method," World Scientific Publishing Co. Pte. Ltd, 2003.

[2] "ANSYS 14.5 Help," *ANSYS, Inc*, Southpointe, 275 Technology Drive, Canonsburg, PA 15317.

[3] Wie, B. "Hypervelocity Nuclear Interceptors for Asteroid Disruption," Acta Astronautica, 90, 2013, pp. 146-155.

[4] Pitz, A., Kaplinger, B., Vardaxis, G., Winkler, T., & Wie, B., "Conceptual Design of a Hypervelocity Asteroid Intercept Vehicle (HAIV) and Its Flight Validation Mission," Acta Astronautica, 94, 2014, pp 42-56.

[5] Barbee, B., Wie, B., Steiner, M., & Getzandanner, K., "Conceptual Design of HAIV Flight Demonstration Mission," AIAA-2013-4544, AIAA Guidance, Navigation, and Control Conference, Boston, MA, August 19-22, 2013.

[6] Kaplinger, B., Premaratne, P.D., Setzer, C., & Wie, B., "GPU-Accelerated 3D Modeling and Simulation of a Blended Kinetic Impact and Nuclear Subsurface Explosion," AIAA-2013-4548, AIAA Guidance, Navigation, and Control Conference, Boston, MA, August 19-22, 2013.

[7] Marinova, M.M., Aharonson, O., Asphaug, E., "Geophysical Consequences of Planetary-Scale Impacts into a Mars-like Planet",*Icarus*,Vol. 211, 2011, pp. 960-985.

[8] "The Military Critical Technologies List (Part II)," Department of Defense,1400 Defense Pentagon, Washington, DC 20301, 1998.

[9] Gurjicic, M., Pandurangan, B., & Cheeseman, B.A., "A Computational Analysis of Detonation of Buried Mines."*Multidiscipline Modeling in Materials and Structures*, Vol. 2, 2006, pp 363-388.

[10] "Effects of Nuclear Earth-Penetrator and Other Weapons," National Academy of Sciences, 2005.

[11] Zhang, A., Yang, W., Huang, C., Ming, F., "Numerical simulation of column charge underwater explosion based on SPH and BEM combination",*Computers and Fluids*, Vol. 71, 2013, pp. 169-178.

[12] Huynh, H. T., A Flux Reconstruction Approach to High-Order Schemes Including Discontinuous Galerkin Methods. *AIAA*, 2007-4079, 2007.

[13] Bassi, F. & Rebay. S., High-Order Accurate Discontinuous Finite Element Solution of the 2D Euler Equations. *Journal of Computational Physics*, *138*, 251–285, 1997.

[14] Baumann, C. E., & Oden. T. J., A Discontinuous Hp Finite Element Method for the Euler and Navier-Stokes Equations. *International Journal for Numerical Methods in Fluids*, *31*(1), 79–95, 1999.

[15] Wang, Z. J., *Adaptive High-Order Methods in Computational Fluid Dynamics*, Ch.15, P. 424, 2011.

[16] Cockburn. B., & Shu. C. W., The Runge-Kutta Discontinuous Galerkin Method for Conservation Laws V: Multidimensional Systems. *Journal of Computational Physics*, *141*, 199–224, 1998.

[17] Kopriva., D. A. & Kolias. J. H., A Conservative Staggered-Grid Chebyshev Multidomain Method for Compressible Flows. *Journal of Computational Physics*, *125*, 244, 1996.

[18] Kopriva. D. A., A Staggered-Grid Multidomain Spectral Method for the Compressible Navier-Stokes Equations. *Journal of Computational Physics*, *143*, 125–158, 1998.

[19] Liu. Y., Vinokur. M., & Wang. Z. J., Three-Dimensional High-Order Spectral Finite Volume Method for Unstructured Grids, *AIAA*, 2003-3837, 2003.

[20] Liu. Y., Vinokur. M., & Wang. Z. J., Discontinuous Spectral Difference Method for Conservation Laws on Unstructured Grids *Journal of Computational Physics*, *216*, 780–801, 2006.

[21] Sun. Y. & Wang. Z. J., High-Order Multidomain Spectral Difference Method for the Navier-Stokes Equations on Unstructured Hexahedral Grids. *Journal of Computational Physics*, *2*(2), 301–333, 2007.

[22] Wang. Z. J., Spectral (Finite) Volume Method for Conservation Laws on Unstructured Grids: Basic Formulation. *Journal of Computational Physics* , *178*, 210–251, 2002.

[23] Zimmerman. B. J. & Wang. Z. J., The Efficient Implementation of Correction Procedure Via Reconstruction with GPU Computing. *AIAA* , 2013-2692, 2013.

[24] Persson. P. O. & Peraire. J., Sub-Cell Shock Capturing for Discontinuous Galerkin Methods. *AIAA* 2006-112, 2006.

[25] P. Woodward, P Colella, The Numerical Simulation of Two-Dimensional Fluid Flow with Strong Shocks *Journal of Computational Physics*, *54*, 115–173, 1984.